6246 *Chem. Mater.* **2010,** *22,* 6246–6253
DOI:10.1021/cm101665r

CHEMISTRY OF MATERIALS
Article

Behavior of Ba(Co, Fe, Nb)$O_{3-\delta}$ Perovskite in CO_2-Containing Atmospheres: Degradation Mechanism and Materials Design

Jianxin Yi,*,† Michael Schroeder,*,† Thomas Weirich,‡,§ and Joachim Mayer‡

†*Institute of Physical Chemistry, RWTH Aachen University, Landoltweg 2, 52056 Aachen, Germany,* ‡*Central Facility for Electron Microscopy, RWTH Aachen University, Ahornstrasse 55, 52074 Aachen, Germany, and* §*Institute of Crystallography, RWTH Aachen University, Jaegerstrass 17-19, 52066 Aachen, Germany*

Received June 15, 2010. Revised Manuscript Received October 5, 2010

This study investigates the degradation behavior and mechanism of perovskite-type $BaCo_{0.4}Fe_{0.4}Nb_{0.2}O_{3-\delta}$ membranes in CO_2-containing atmospheres at 800−1000 °C and examines the influence of cation substitution on the CO_2 resistance. The oxygen permeation flux deteriorates rapidly upon switching the sweep gas from Ar to CO_2. During exposure to CO_2, the membrane material decomposes to form a compact $BaCO_3$ surface layer and a subjacent porous decomposed zone which consists of CoO and a Co-depleted Ba(Co, Fe, Nb)$O_{3-\delta}$ perovskite phase. Within this zone, the composition of the perovskite product varies with depth, with more pronounced cobalt depletion found closer to the carbonate layer. The growth of the product layers is found to be diffusion-controlled and can be enhanced by the presence of oxygen. Outward diffusion of barium from the unreacted perovskite bulk appears to rate limit the growth. A drop of the barium chemical potential is concurrent with a larger degree of cobalt depletion in the Ba(Co, Fe, Nb)$O_{3-\delta}$ phase. This suggests that Co substitution by Fe, or particularly by Nb, results in better CO_2 resistance. The effectiveness of the Fe/Nb substitution was experimentally proved and may be ascribed to increase in both the oxygen stoichiometry and acidity of the perovskite. A strategy for development of CO_2-resistant materials is then proposed.

1. Introduction

In recent years, increasing attention has been drawn to mixed ionic-electronic conducting perovskite oxides (MIEC), due to their potential application as materials for oxygen permeable membranes[1−3] and for cathode of solid oxide fuel cells (SOFC).[4] Dense MIEC ceramic membranes are able to separate oxygen from air at high temperatures with high oxygen permeability and infinite selectivity. In a power plant with integrated carbon capture and storage technology, MIEC membranes may be utilized to provide pure oxygen for the fuel combustion (oxy-fuel process).[5,6] The resulting flue gas is free of nitrogen, which greatly facilitates the sequestration of carbon dioxide. If employed in a sweep gas driven oxy-fuel process (4-end process), the membrane is exposed to a recirculated sweep gas stream to pick up any permeated oxygen.[6] As the flue gas contains highly concentrated carbon dioxide, stability of the membrane against corrosion of this acidic gas is essential to guarantee long-term operation of the membrane module. However, this poses a great challenge to the highly permeable perovskite membranes, which usually contain significant amounts of basic elements such as alkaline earth metals.

Many MIEC have been shown to be susceptible to the presence of CO_2.[7−21] Deterioration of the oxygen permeation flux upon exposure to CO_2-containing atmospheres

*To whom correspondence should be addressed. Tel: +49-241-809-8622 (J.Y.), +49-241-809-4714 (M.S.). Fax: +49-241-809-2128 (J.Y.), +49-241-809-2128 (M.S.). E-mail: jyi@pc.rwth-aachen.de (J.Y.), schroeder@rwth-aachen.de (M.S.).

(1) Wang, H. H.; Werth, S.; Schiestel, T.; Caro, A. *Angew. Chem., Int. Ed.* **2005**, *44*, 6906.
(2) Bouwmeester, H. J. M.; Burggraaf, A. J. In *CRC Handbook of Solid State Electrochemstry*; Gellings, P. J., Bouwmeester, H. J. M., Eds.; CRC Press: Boca Raton, FL, 1997; pp 481.
(3) Chen, C. S.; Feng, S. J.; Ran, S.; Zhu, D. C.; Liu, W.; Bouwmeester, H. J. M. *Angew. Chem., Int. Ed.* **2003**, *42*, 5196.
(4) Shao, Z. P.; Haile, S. M. *Nature* **2004**, *431*, 170.
(5) Griffin, T.; Sundkvist, S. G.; Asen, K.; Bruun, T. *J. Eng. Gas Turbines Power Trans. ASME* **2005**, *127*, 81.
(6) Engels, S.; Beggel, F.; Modigell, M.; Stadler, H. *J. Membr. Sci.* **2010**, *359*, 93.
(7) Yi, J. X.; Feng, S. J.; Zuo, Y. B.; Liu, W.; Chen, C. S. *Chem. Mater.* **2005**, *17*, 5856.
(8) Yaremchenko, A. A.; Kharton, V. V.; Avdeev, M.; Shaula, A. L.; Marques, F. M. B. *Solid State Ionics* **2007**, *178*, 1205.
(9) Homonnay, Z.; Nomura, K.; Juhasz, G.; Gal, M.; Solymos, K.; Hamakawa, S.; Hayakawa, T.; Vertes, A. *Chem. Mater.* **2002**, *14*, 1127.
(10) Carolan, M. F.; Dyer, P. N.; LaBar, S.; M., J.; Thorogood, R. M. U.S. Patent 5240473, 1993.
(11) Benson, S. J.; Waller, D.; Kilner, J. A. *J. Electrochem. Soc.* **1999**, *146*, 1305.
(12) Tong, J. H.; Yang, W. S.; Zhu, B. C.; Cai, R. *J. Membr. Sci.* **2002**, *203*, 175.
(13) Arnold, M.; Wang, H. H.; Feldhoff, A. *J. Membr. Sci.* **2007**, *293*, 44.
(14) Martynczuk, J.; Efimov, K.; Robben, L.; Feldhoff, A. *J. Membr. Sci.* **2009**, *344*, 62.
(15) Kaus, I.; Wiik, K.; Krogh, B.; Dahle, M.; Hofstad, K. H.; Aasland, S. *J. Am. Ceram. Soc.* **2007**, *90*, 2226.
(16) Waindich, A.; Mobius, A.; Muller, M. *J. Membr. Sci.* **2009**, *337*, 182.
(17) Yang, Z.; Harvey, A. S.; Gauckler, L. J. *Scr. Mater.* **2009**, *61*, 1083.
(18) Yan, A. Y.; Maragou, V.; Arico, A.; Cheng, M.; Tsiakaras, P. *Appl. Catal. B, Environ.* **2007**, *76*, 320.

 Published on Web 10/28/2010 © 2010 American Chemical Society

has been reported for a number of different compositions, including $Sr(Co, Fe)O_{3-\delta}$,[7-9] $(La, Sr)(Co, Fe)O_{3-\delta}$,[10,11] Zr-doped $Ba(Co, Fe)O_{3-\delta}$,[12] $Ba_{0.5}Sr_{0.5}Co_{0.8}Fe_{0.2}O_{3-\delta}$ (BSCF),[13] and $(Ba, Sr)(Zn, Fe)O_{3-\delta}$ (BSZF).[14] Arnold et al. observed instant cessation of the oxygen permeation process when subjecting a BSCF membrane to a pure CO_2 sweep gas stream at 875 °C. After exposure, a surface carbonate layer and an adjacent intermediate layer of complex structure were observed on the surface of the BSCF, and the carbonate formation was proposed to be responsible for degradation of the membrane performance.[13] Recently, Martynczuk et al. reported that formation of a small amount (8%) of carbonate on the surface of a BSZF membrane is sufficient to result in rapid breakdown of the oxygen permeability at 750 °C in a CO_2 atmosphere.[14] Similarly, the electrical performance of SOFC cathodes consisting of BSCF was also found to be very sensitive to the presence of CO_2 in the cathode surroundings.[18] Degradation was observed even in a 1% CO_2/O_2 mixture and at a temperature as low as 450 °C.[18] Furthermore, degradation of the hydrogen permeability and structure of $BaCeO_3$-based perovskite-type proton conductors in CO_2 has also been reported.[22-25] However, a comprehensive understanding of the degradation process and mechanism for the perovskite membranes in CO_2 is still lacking.

A few experimental attempts have been reported to improve the CO_2 resistance of perovskite MIEC by proper cation substitution.[22,23,26] Zeng et al.[26] discovered that Ti substitution for Co and Fe in $SrCo_{0.8}Fe_{0.2}O_{3-\delta}$ (SCF) perovskite greatly improves the CO_2 tolerance. At 950 °C and in contact with CO_2 as sweep gas, SCF doped with 10−20 mol % Ti displayed no deterioration of the oxygen permeability within 80 h, in contrast to a drop of 70% for the undoped SCF. On the other hand, improvement of the chemical stability in CO_2 for $BaCeO_3$-based materials has also been achieved by partial substitution of Zr for Ce.[22,23] Nevertheless, the reason why such cation substitution improves the CO_2 resistance is not yet clear. The effectiveness of Zr doping in $BaCeO_3$ is well consistent with some reported thermodynamic analyses.[22,27] However, such thermodynamic analyses face difficulty in dealing with nonstoichiometric perovskite oxides such as the aforementioned Ti-doped SCF, because of the unavailability of their thermodynamic data. The better CO_2 resistance due to Ti doping in SCF was attributed by Zeng et al. to the higher bond energy of the Ti−O bond than those of the Fe−O and Co−O bonds, which lowers the material's basicity.[26] Nevertheless, since the bond energy of Zr−O (760 kJ/mol) is smaller than that of Ce−O (795 kJ/mol), the improved CO_2 resistance by Zr doping in $BaCeO_3$ cannot be accounted for by the bond energy difference. Exploration of CO_2-resistant oxygen permeable peorvskite membranes for the oxy-fuel process urges better understanding of their behavior in CO_2.

Recently, Nb was found to be able to enhance the stability while maintaining a high oxygen permeability of $SrCoO_{3-\delta}$-based perovskite.[28] Nb-doped $Ba(Co,Fe)O_{3-\delta}$ perovskite was also reported to exhibit a high oxygen permeation flux and good phase stability in a reducing atmosphere,[29,30] which may be a candidate as an oxygen permeable membrane for oxy-fuel combustion. In this work, we use $BaCo_{0.4}Fe_{0.4}Nb_{0.2}O_{3-\delta}$ as a model material to investigate the oxygen permeation performance and (micro)structural behavior of perovskite membranes in CO_2-containing atmospheres. Furthermore, the effect of variation of iron and niobium content on the permeation property and stability of the material is also examined.

2. Experimental Section

$BaCo_{1-x-y}Fe_xNb_yO_{3-\delta}$ (x = 0.2−0.8, y = 0.2−0.5) powders were synthesized by a conventional solid state reaction method. Appropriate amounts of $BaCO_3$, Co_3O_4, Fe_3O_4 (or Fe_2O_3), and Nb_2O_5 were weighed according to the cation stoichiometry and thoroughly mixed. Powder calcination was carried out at 1050 °C and then 1100 °C for 15 h, respectively. Sintering was performed in air for a period of 10 h at 1200 °C for the Co-containing compositions or at 1350 °C for the Co-free compositions. Polished pellets and powders from crushing the sintered ceramics were pre-equilibrated in air or a flowing Ar/O_2 mixture, annealed in CO_2-containing gas streams at 900 °C, and subsequently quenched to room temperature in the same atmosphere (see Supporting Information for details).

Phase analysis was conducted by means of X-ray diffraction (XRD, STOE STADI-P transmission diffractometer, and STOE Theta−Theta reflection diffractometer). Indexing and lattice parameter refinement was performed using a Werner's TREOR program (STOE WinXPOW). The microstructure of the disk-shaped samples was examined both prior to and after annealing by various techniques including scanning electron microscopy (SEM, LEO 1450VP), energy-dispersive X-ray microanalysis (EDS, Oxford INCA and EDAX), scanning-transmission electron microscopy (STEM, FEI Tecnai F20), selected area electron diffraction (SAED), and electron energy loss spectroscopy (EELS, Gatan GIF 2000). To study the formation of new phases formed during the annealing, a thin lamella was cut from the sample surface by means of a focused ion beam (FIB, FEI Strata 205). The lamella was then investigated by transmission electron microscopy.

Oxygen permeation measurements were conducted with a homemade setup. A disk-shaped membrane was positioned between two alumina tubes and sealed to gas-tightness by gold

(19) Bucher, E.; Egger, A.; Caraman, G. B.; Sitte, W. *J. Electrochem. Soc.* **2008**, *155*, B1218.
(20) Tarancon, A.; Penamartinez, J.; Marrerolopez, D.; Morata, A.; Ruizmorales, J.; Nunez, P. *Solid State Ionics* **2008**, *179*, 2372.
(21) Yang, Q.; Lin, Y. S. *Ind. Eng. Chem. Res.* **2006**, *45*, 6302.
(22) Ryu, K. H.; Haile, S. M. *Solid State Ionics* **1999**, *125*, 355.
(23) Zuo, C. D.; Dorris, S. E.; Balachandran, U.; Liu, M. L. *Chem. Mater.* **2006**, *18*, 4647.
(24) Chen, F. L.; Sorensen, O. T.; Meng, G. Y.; Peng, D. K. *J. Mater. Chem.* **1997**, *7*, 481.
(25) Zakowsky, N.; Williamson, S.; Irvine, J. T. S. *Solid State Ionics* **2005**, *176*, 3019.
(26) Zeng, Q.; Zu, Y. B.; Fan, C. G.; Chen, C. S. *J. Membr. Sci.* **2009**, *335*, 140.
(27) Yokokawa, H.; Sakai, N.; Kawada, T.; Dokiya, M. *Solid State Ionics* **1992**, *52*, 43.
(28) Nagai, T.; Ito, W.; Sakon, T. *Solid State Ionics* **2007**, *177*, 3433.
(29) Cheng, Y.; Zhao, H.; Teng, D.; Li, F.; Lu, X.; Ding, W. *J. Membr. Sci.* **2008**, *322*, 484.
(30) Harada, M.; Domen, K.; Hara, M.; Tatsumi, T. *Chem. Lett.* **2006**, *35*, 1326.

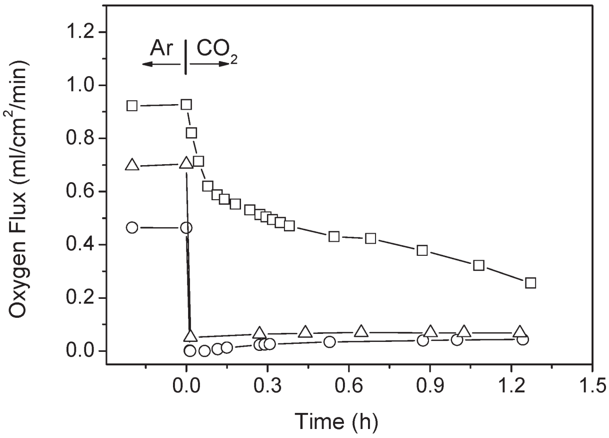

Figure 1. Time dependence of oxygen permeation flux of a 1 mm thick $BaCo_{0.4}Fe_{0.4}Nb_{0.2}O_{3-\delta}$ membrane with CO_2 as sweep gas at (□) 1000 °C, (△) 900 °C, and (○) 800 °C.

rings. During the permeation measurements, synthetic air and Ar/CO_2 (or He/CO_2) mixtures were fed to the feed side and sweep side of the membrane, respectively. Composition of the permeate effluent was analyzed by a calibrated Balzers OmniStar mass spectrometer or Agilent 7890A gas chromatograph.

3. Results

3.1. Oxygen Permeation. The permeation fluxes obtained from a $BaCo_{0.4}Fe_{0.4}Nb_{0.2}O_{3-\delta}$ (BCFN442) membrane with pure Ar or CO_2 as sweep gas are shown in Figure 1. Upon switching the sweep gas from Ar to CO_2 at temperatures of 800 and 900 °C, the oxygen flux dropped almost instantaneously to a negligible level. At a higher temperature of 1000 °C, introduction of CO_2 led to a quick initial drop of the oxygen flux, followed by a further slow decrease. When the CO_2 partial pressure in the sweep gas was lowered from 1 to 0.33 bar, degradation of the oxygen permeation flux became less pronounced (see Supporting Information, Figure S1).

3.2. Phase Composition. In order to better understand why the oxygen permeation process broke down in the presence of CO_2, BCFN442 powder samples were annealed at 900 °C in flowing CO_2 for different periods of time and studied by XRD. Analysis of the XRD patterns (Figure 2) revealed that part of the reflections can be attributed to $BaCO_3$ and CoO and that the residual reflections can be indexed as a cubic structure. The lattice constants of the cubic phases, varying in the range of 0.405−0.406 nm, are slightly smaller than that (a = 0.407 nm) of the as-prepared BCFN442. This suggests that a perovskite-structured phase with modified composition was formed during the annealing. Formation of $BaCO_3$ can be observed even after a CO_2 exposure time as short as 3 min (Figure 2b); however, the perovskite peaks are broadened and even split, which may be due to distortion of the structure in this sample. In order to track the progress of the reaction between BCFN442 and CO_2, the intensities of both the $BaCO_3$ (111) and CoO (200) reflections were normalized to that of the perovskite (110) reflection. Both normalized intensities increase rapidly within an annealing time of 24 h and then level off (see Supporting Information, Figure S2).

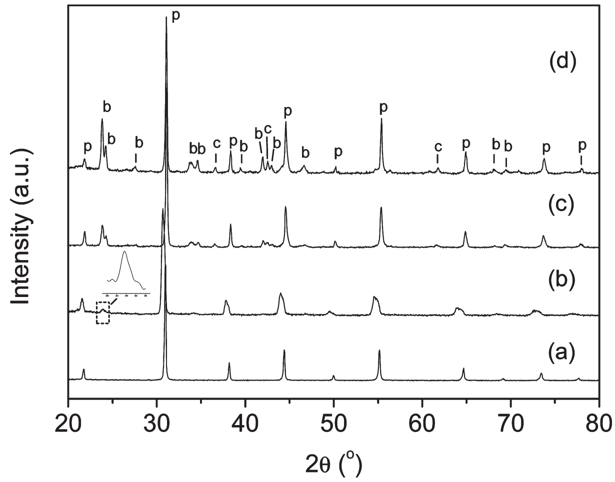

Figure 2. X-ray diffraction pattern for $BaCo_{0.4}Fe_{0.4}Nb_{0.2}O_{3-\delta}$ powders treated under various conditions. (a) Crushed powder from an as-sintered pellet; (b−d) annealed at 900 °C in CO_2 for (b) 3 min, (c) 2 h, and (d) 240 h. p: perovskite; b: $BaCO_3$ (JCPDS 71-2394); c: CoO (JCPDS 70-2856).

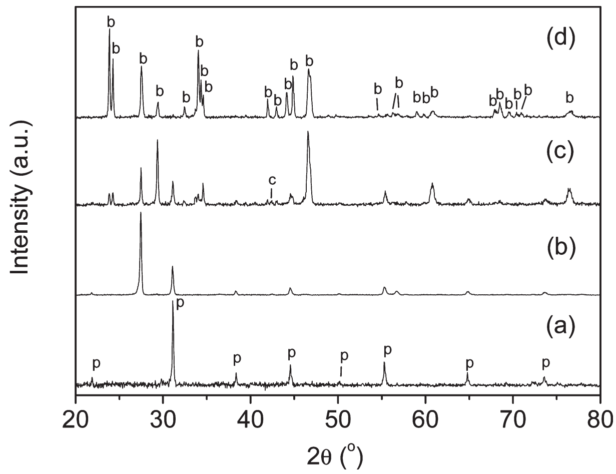

Figure 3. X-ray diffraction pattern for $BaCo_{0.4}Fe_{0.4}Nb_{0.2}O_{3-\delta}$ pellets annealed in CO_2 at 900 °C for (a) 3 min, (b) 2 h, (c) 24 h, and (d) 240 h. p: perovskite; b: $BaCO_3$ (JCPDS 71-2394); c: CoO (JCPDS 70-2856).

For a comparison, BCFN442 pellet samples were annealed under the same conditions as the powder samples and examined with XRD (Figure 3). After an annealing time of 3 min, only reflections from the perovskite phase were observed. As the annealing time increases (within 24 h), both $BaCO_3$ and small amounts of CoO were detected in addition to the perovskite phase. However, the intensity of the $BaCO_3$ peaks relative to that of its (111) peak, differs from that for the annealed powders shown in Figure 2, indicating that $BaCO_3$ crystallites grow with a preferred orientation in the initial stages of formation. Upon further prolongation of the annealing time to 240 h, reflections from CoO and from the cubic phase disappear and only those from $BaCO_3$ were detected.

3.3. Microstructure. Figure 4 shows a series of SEM micrographs taken from membrane surfaces that were annealed in CO_2 at 900 °C. After an annealing time of 3 min, small particles of a secondary phase are observed, which grow to form a compact and continuous layer covering the sample surface after 2 h.

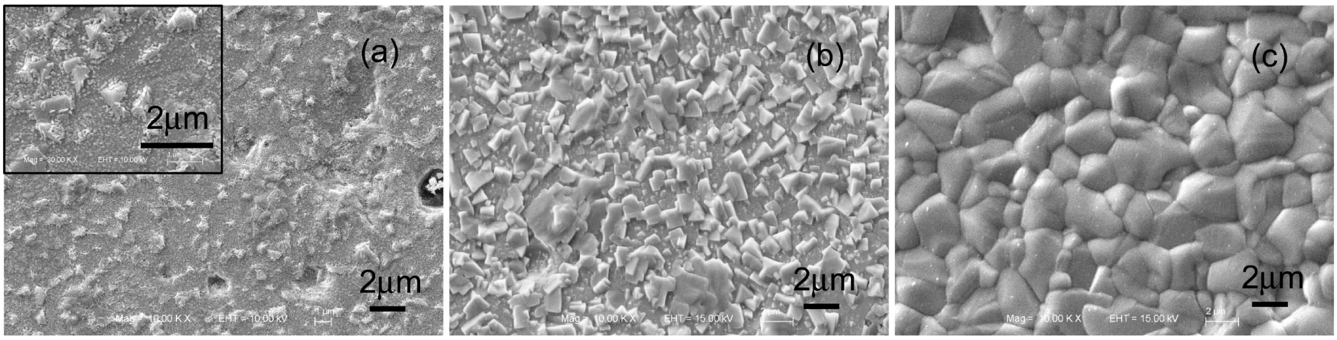

Figure 4. SEM images taken from the surface of $BaCo_{0.4}Fe_{0.4}Nb_{0.2}O_{3-\delta}$ membranes exposed to CO_2 at 900 °C for (a) 3 min, (b) 0.5 h, and (c) 2 h. The inset in (a) shows a zoom of the microstructure.

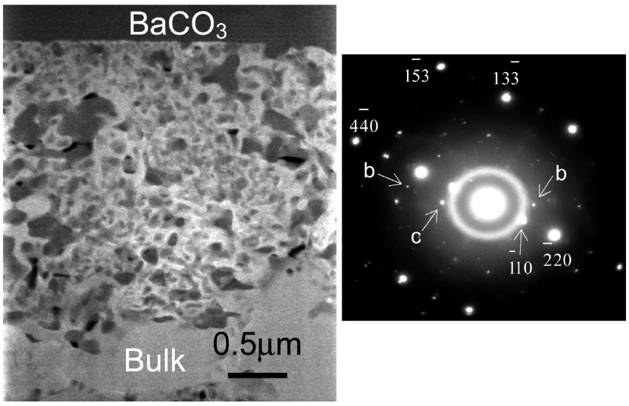

Figure 5. Scanning TEM high-angle annular dark field (STEM HAADF) micrograph (left) of a lamella featuring the near-surface region of a $BaCo_{0.4}Fe_{0.4}Nb_{0.2}O_{3-\delta}$ membrane exposed to CO_2 at 900 °C for 2 h. The electron diffraction pattern at the right was taken from the intermediate decomposed zone, along the [334] zone axis of the perovskite phase. b and c represent $BaCO_3$ and CoO phase, respectively.

A FIB lamella representing the cross section of the near-surface region of the 2 h-annealed membrane was studied by TEM-EDS and EELS. The high-resolution EDS measurements confirmed that the newly formed surface layer consists only of Ba, C, and O (see Supporting Information, Figure S3a). The EELS pattern revealed a prepeak of the carbon K-edge at ~284 eV, which is characteristic for conjugated π electron systems, e.g., the flat CO_3 anion present in $BaCO_3$ (see Supporting Information, Figure S3b). Therefore, the new surface layer can be ascribed to $BaCO_3$. The carbonate layer and the dense bulk are separated by a porous zone, where decomposition has led to formation of fine particles of two different phase contrasts (Figure 5). Semiquantitative elemental analysis showed that the less abundant darker phase corresponds to $BaCO_3$, whereas the brighter phase consists of all constituent elements of Ba(Co, Fe, Nb)$O_{3-\delta}$. The latter phase is significantly depleted of Co and enriched in Fe and Nb in comparison with the bulk composition (Table 1). We note, however, that the bulk composition determined by EDS also shows a slight local variation. SAED analysis (Figure 5) of the decomposed zone revealed the main phase to be in a cubic structure having a lattice constant of 0.406 nm, which is thus assigned to the Co-depleted Ba(Co, Fe, Nb)$O_{3-\delta}$ perovskite phase in line with the aforementioned XRD results.

Table 1. TEM-EDX Data (in at %) of the Perovskite Phase at Various Sample Depths[a] in the Decomposed Zone of a $BaCo_{0.4}Fe_{0.4}Nb_{0.2}O_{3-\delta}$ Membrane Exposed to CO_2 at 900 °C for 2 h

	depth (μm)	Fe	Co	Nb	Ba
decompose 1	0.5	27.9	1.2	30.7	40.3
decompose 2	1.0	31.4	2.8	25.5	40.2
bulk 1	2.9	23.1	20.6	17.1	39.1
bulk 2	6.6	24.3	22.6	13.9	39.1

[a] The sample depth starts from the boundary between the carbonate layer and decomposed zone and extends to the bulk.

On the other hand, both $BaCO_3$ and CoO are also identified as minor phases in the decomposed zone, leaving one weak reflection at $d = 0.57$ nm in the SAED pattern unindexed.

Similar microstructural changes were observed in BCFN442 membranes annealed in CO_2 for a longer time at 900 °C. Figure 6 shows a SEM micrograph and the elemental distribution of the cross section of a membrane exposed to CO_2 at 900 °C for 240 h. At a small depth ($< \sim 10-20\,\mu$m) in the decomposed zone, the porosity was found to be significantly higher than at larger depths. Comparison of the SEM micrograph and the X-ray maps show that two phases of different composition can be distinguished. A dark phase, which is significantly enriched with Co and depleted of the other three cations, is predominantly abundant in the highly porous region. At larger sample depth, the dark phase exhibits bigger grain sizes and appears to be located at the grain boundaries of the brighter phase. The dark phase contains more than 97 at % Co in the overall cation composition and, hence, can be assigned to the CoO phase which was already identified by both XRD and SAED. In contrast, the bright phase contains all four cations of the parent compound but is significantly depleted of Co and, thus, corresponds to the Co-depleted Ba(Co, Fe, Nb)$O_{3-\delta}$ perovskite. The quantitative cation composition for this Ba(Co, Fe, Nb)$O_{3-\delta}$ perovskite was also determined and plotted in Figure 7 against the sample depth which extends from the boundary between the carbonate layer and the decomposed zone to the bulk. Within experimental errors, the content of the A-site cation, Ba, as well as the A/B (B = Co, Fe, Nb) ratio (see Supporting Information, Figure S4), remains constant. However, the contents of the B-site cations vary with the sample depth and exhibit a significant deviation from their nominal

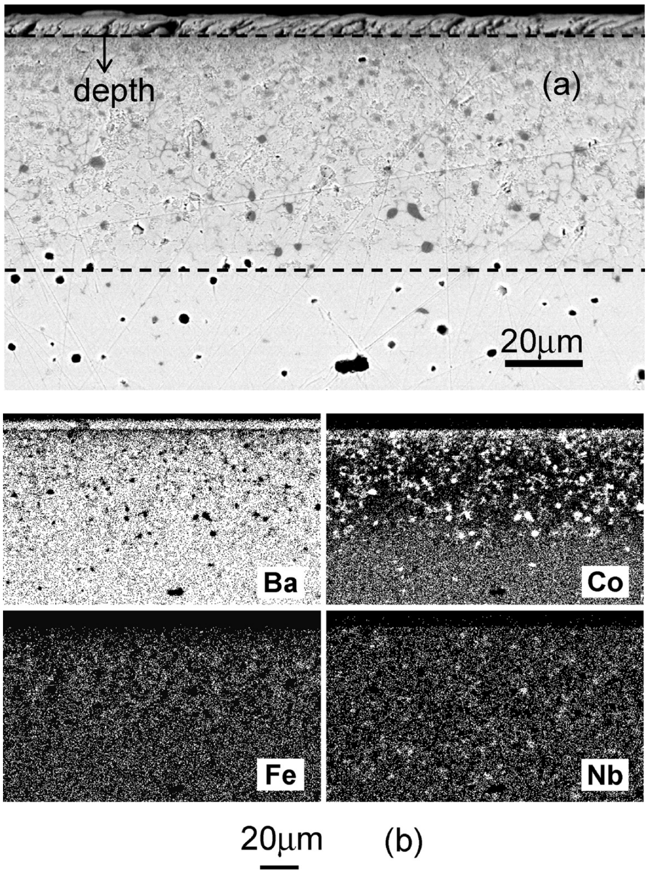

Figure 6. (a) Back scattered electron image and (b) elemental mapping of the cross section of a $BaCo_{0.4}Fe_{0.4}Nb_{0.2}O_{3-\delta}$ membrane that was polished after being annealed in CO_2 for 240 h at 900 °C.

values close to the carbonate layer. As the sample depth increases, both the Fe and Nb contents decrease, whereas the Co content increases. Unlike the 2 h-annealed sample, no $BaCO_3$ formation was observed in the decomposed zone of the long-term annealed membrane.

3.4. Degradation Kinetics. The thickness of both the carbonate surface layer and decomposed zone increases with the CO_2 annealing time, the latter being around 10 times thicker than the former. The growth of the layers can be approximated by a simple parabolic rate law (Figure 8), indicating a diffusion-controlled process.[31]

It was also found that the growth kinetics depends significantly on the partial pressures of CO_2 (pCO_2) and O_2 (pO_2) in the surrounding gas. After a 24 h anneal at 900 °C, the thickness of the product layers is over 30% smaller for the annealing atmosphere of 33% CO_2/Ar (pCO_2 = 0.33 bar) than for pure CO_2 (pCO_2 = 1 bar). On the other hand, when the gas composition was changed from 33% CO_2/Ar to 33% CO_2/O_2, corresponding to an increase of pO_2 from below $\sim 10^{-5}$ bar to 0.67 bar, over an 80% increment in the product thickness was observed after 24 h at 900 °C. It is noteworthy that the diffusion-controlled mechanism for the growth of the product layers remains valid in the high pO_2 region (Figure 8).

In order to gain more insight into the diffusion-controlled process, the surface of a BCFN442 pellet was

(31) Schmalzried, H. *Chemical Kinetics of Solids*; VCH: Weinheim: 1995.

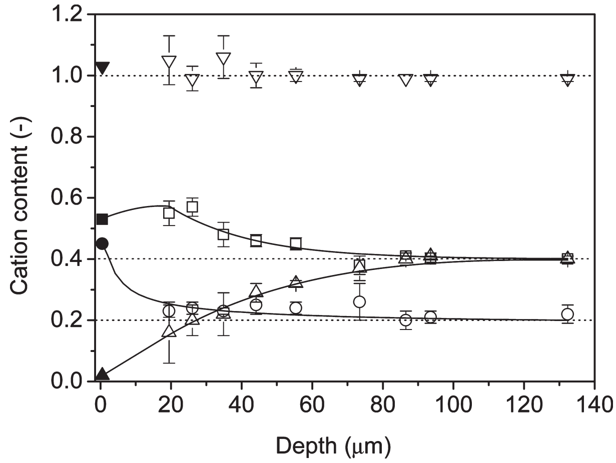

Figure 7. Variation of the cation contents of the perovskite phase with the sample depth obtained by SEM-EDX for a $BaCo_{0.4}Fe_{0.4}Nb_{0.2}O_{3-\delta}$ membrane after being annealed in CO_2 for 240 h at 900 °C: (▽) Ba, (△) Co, (□) Fe, and (○) Nb. The sample depth extends from the boundary between the carbonate layer and decomposed zone to the bulk, as illustrated in Figure 6a. The cation contents were obtained by normalizing the measured atomic percentage of each individual cation to that of an untreated $BaCo_{0.4}Fe_{0.4}Nb_{0.2}O_{3-\delta}$ reference sample, taking into account their respective nominal fractions; e.g., for Co, it is $(Co\%^{Ba(Co,Fe,Nb)O_{3-\delta}})/(Co\%^{BCFN442}) \times 0.4$. For comparison, the data in the near-surface region of the 2 h-annealed sample obtained by TEM-EDX as given in Table 1 are also presented (filled symbols). Solid lines are guides to the eye, whereas dashed lines indicate the reference values for the respective cations.

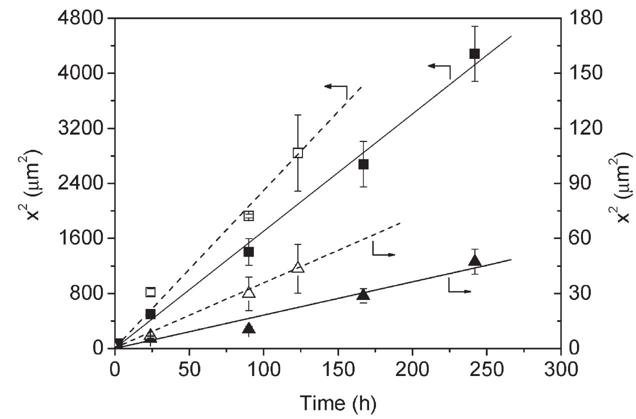

Figure 8. Parabolic plot of the thickness for the decomposed zone (square) and $BaCO_3$ top layer (triangle) versus annealing time for $BaCo_{0.4}Fe_{0.4}$-$Nb_{0.2}O_{3-\delta}$ membrane in CO_2 (filled symbols) or 33% CO_2/O_2 (open symbols) at 900 °C. Lines are guides to the eye.

sputtered with gold and then exposed to CO_2 at 900 °C. After the annealing, the gold particles, being an immobile marker, turned out to be embedded at the interface between the $BaCO_3$ layer and decomposed zone (Figure 9). This observation unambiguously indicates that $BaCO_3$ grew outward at the outer surface of the membrane.

3.5. Cation Substitution. The influence of cation composition on the CO_2 resistance of the perovskite material was also investigated. Oxygen permeation fluxes of a series of $BaCo_{1-x-y}Fe_xNb_yO_{3-\delta}$ (x = 0.2−0.8, y = 0.2−0.5) membranes were measured at 900 °C. Similar to BCFN442, the oxygen flux for the samples decreased quickly upon exposure to CO_2. Results at a measuring time of 1 h are shown in Figure 10. It is evident that, with increasing iron content in $BaCo_{1-x-y}Fe_xNb_yO_{3-\delta}$ (x = 0.2−0.8, y = 0.2),

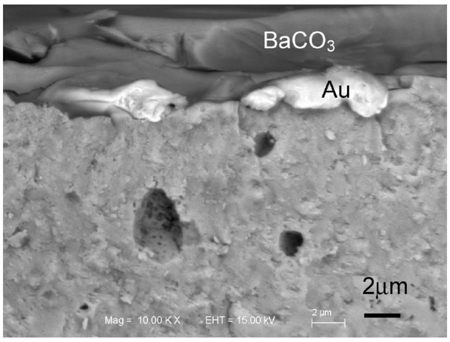

Figure 9. Back scattered electron image of a fractured $BaCo_{0.4}Fe_{0.4}Nb_{0.2}O_{3-\delta}$ membrane which was premarked with Au and subjected to annealing in CO_2 at 900 °C for 90 h.

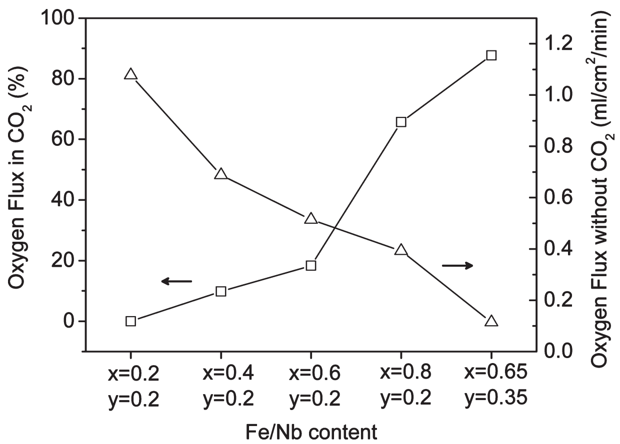

Figure 10. Oxygen permeation flux of $BaCo_{1-x-y}Fe_xNb_yO_{3-\delta}$ membranes as a function of Fe and Nb content at 900 °C: (△) using CO_2-free sweep gas; (□) after switching the sweep gas to CO_2 for 1 h; the values are normalized to that obtained in Ar (or He) prior to CO_2 introduction. Thickness of the membranes is 1 mm except for $BaFe_{0.65}Nb_{0.35}O_{3-\delta}$ (0.85 mm).

the adverse effect of CO_2 on the oxygen permeability becomes less pronounced. For the cobalt-free composition $BaFe_{0.8}Nb_{0.2}O_{3-\delta}$, a decrease of oxygen flux by 35% was observed, in contrast to a 90% decrease for BCFN442. The decrease of oxygen flux caused by CO_2 reduces to 12% for $BaFe_{0.65}Nb_{0.35}O_{3-\delta}$ ($x = 0.65$, $y = 0.35$), when the Fe in $BaFe_{0.8}Nb_{0.2}O_{3-\delta}$ ($x = 0.8$, $y = 0.2$) is partially substituted by Nb. With Nb content increasing to 0.5 (i.e., $BaFe_{0.5}Nb_{0.5}O_{3-\delta}$), however, no oxygen permeating from the membrane was observed even using Ar as sweep gas at 1000 °C. Despite the complete loss of oxygen permeability in $BaFe_{0.5}Nb_{0.5}O_{3-\delta}$, no structural degradation or $BaCO_3$ formation was observed in the sample annealed in CO_2 at 900 °C for 90 h (see Supporting Information, Figure S5). It is also evident in Figure 10 that the improvement of CO_2 resistance due to substitution of Co by Fe, or of Fe by Nb, unfortunately comes at the cost of a reduced pristine oxygen flux when argon is used as sweep gas.

4. Discussion

4.1. Degradation Mechanism. The BCFN442 perovskite membrane decomposes when exposed to CO_2, leading to formation of $BaCO_3$ on the surface and an underneath porous structure mainly consisting of a Co-depleted Ba(Co, Fe, Nb)$O_{3-\delta}$ phase and CoO. After the $BaCO_3$ particles grow into a continuous layer, the degradation process is characterized by a slow diffusion-controlled growth of the product layers.

The outward growth of the $BaCO_3$ surface layer clearly indicates that this layer is formed by diffusion of barium (in the form of Ba^{2+}) from the ceramic bulk to the outer surface rather than transport of CO_2 from the surrounding gas into the solids (Figure 9). The nonporous $BaCO_3$ layer does not seem to allow gaseous CO_2 to penetrate. The minor amount of $BaCO_3$ found in the decomposed zone of the 2 h-annealed sample was likely formed before the continuous $BaCO_3$ layer was established at the surface. The formation of $BaCO_3$ at the gas−solid interface requires oxygen as one of the reactants in addition to Ba^{2+} and CO_2, which may be provided either from the gas phase or from the bulk via solid state diffusion of oxide ions. In the former case, electronic charge carriers are required for charge compensation. The following mechanism may then be assumed for the degradation of BCFN442 in CO_2, which may also be operative in other perovskite membrane materials:[32] (1) Part of Ba^{2+} leaves the BCFN442 perovskite; concurrently, CoO precipitates and a Co-depleted perovskite phase is formed:

$$\begin{aligned} &BaCo_{0.4}Fe_{0.4}Nb_{0.2}O_{3-\delta} \rightarrow mBa^{2+} \\ &+ (1-m)BaCo_{(0.4-y)}Fe_{(0.4+z)}Nb_{(0.2+y-z)}O_{3-\delta'} \\ &+ nCoO + 2me' \end{aligned} \quad (1)$$

(2) Ba^{2+} diffuses through the perovskite product phase in the decomposed zone and, subsequently, through $BaCO_3$ to the gas−solid interface; simultaneously, cocurrent transport of the electrons takes place. (3) Ba^{2+} and the electrons reacts with CO_2 and O_2 at the outer solid surface, resulting in growth of the $BaCO_3$ layer:

$$Ba^{2+} + CO_2(g) + O_2(g) + 2e' \rightarrow BaCO_3(s) \quad (2)$$

The overall reaction is

$$\begin{aligned} &aCO_2 + bO_2 + BaCo_{0.4}Fe_{0.4}Nb_{0.2}O_{3-\delta} \rightarrow aBaCO_3 \\ &+ cCoO + (1-a)BaCo_{(0.4-y)}Fe_{(0.4+z)}Nb_{(0.2+y-z)}O_{3-\delta'} \end{aligned} \quad (3)$$

In case of oxide ions being the predominant oxygen source for the carbonate formation, the overall reaction becomes

$$\begin{aligned} &aCO_2 + BaCo_{0.4}Fe_{0.4}Nb_{0.2}O_{3-\delta} \rightarrow aBaCO_3 + bCoO \\ &+ (1-a)BaCo_{(0.4-y)}Fe_{(0.4+z)}Nb_{(0.2+y-z)}O_{3-\delta'} \end{aligned} \quad (4)$$

The observation that increasing the oxygen partial pressure significantly enhances the membrane degradation seems to favor reaction 3. We note, however, in order to

(32) Yi, J.; Schroeder, M., submitted for publication.

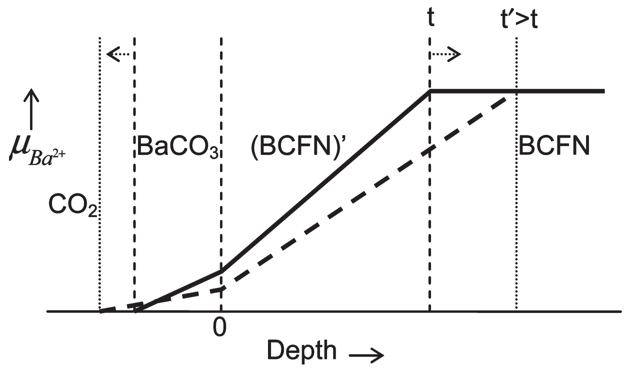

Figure 11. Variation of the chemical potential of Ba^{2+} of the perovskite phase and $BaCO_3$ with sample depth in the degraded membrane. BCFN and (BCFN)' denote $BaCo_{0.4}Fe_{0.4}Nb_{0.2}O_{3-\delta}$, the intact perovskite bulk, and $BaCo_{0.4-x}Fe_{0.4+y}Nb_{0.2+x-y}O_{3-\delta}$, the Co-depleted perovskite product phase in the decomposed zone, respectively. Here, the assumption that the Ba^{2+} diffusion in the decomposed zone takes place mainly through the $BaCo_{0.4-x}Fe_{0.4+y}Nb_{0.2+x-y}O_{3-\delta}$ perovskite is made. The thick line and thick dashed line represent the chemical potential profile at time *t* and *t*', respectively; whereas thin dashed and dotted lines indicate the boundaries of the different zones concerned at time *t* and *t*', respectively.

draw a clear conclusion, further investigation is required to shed more light on the oxygen source for the carbonate formation.

The diffusion-controlled growth of the product layers is expected to be governed by the slow diffusion of Ba^{2+} from the solids to the surface. The diffusion is driven by a gradient of the chemical potential of Ba^{2+} (referred to as $\mu_{Ba^{2+}}$) between the perovskite bulk and the gas–solid interface, as schematically illustrated in Figure 11. Two phenomena are evident from Figure 11. First, at the early stage of the degradation, the chemical potential gradient of Ba^{2+} is so steep that the membrane decomposes seriously, which explains the high porosity and significant CoO precipitation as well as Co depletion in the perovskite phase at a shallow position (< 10–20 μm) in Figure 6. As the product layers become thicker with time, the Ba^{2+} chemical potential gradient gradually flattens out, and as a result, the reaction becomes slower, giving rise to less porosity, less CoO precipitation, and larger CoO grains at a deeper position in the decomposed zone in Figure 6.

Second, the Co-depleted $BaCo_{0.4-y}Fe_{0.4+z}Nb_{0.2+y-z}O_{3-\delta}$ phase was formed in regions of lower chemical potential of barium, which implies that this phase becomes more resistant to CO_2 as Co is replaced by Fe and Fe is replaced by Nb. This hypothesis agrees well with the less susceptibility of the oxygen permeation fluxes of $BaCo_{1-x-y}Fe_xNb_yO_{3-\delta}$ to CO_2 with increasing Fe and Nb content in Figure 10. Although degradation in CO_2 occurs for all the compositions except the nonoxygen-permeable $BaFe_{0.5}Nb_{0.5}O_{3-\delta}$ investigated in this work, a full CO_2-resistant composition that is permeable for oxygen may be achieved at a niobium content between $y = 0.35$ and $y = 0.5$ for the Co-free $BaCo_{1-x-y}Fe_xNb_yO_{3-\delta}$. The undetected oxygen permeation flux of $BaFe_{0.5}Nb_{0.5}O_{3-\delta}$ is probably due to the absence of oxygen vacancy, as niobium and iron are in the valence state of 5+ and 3+,[33,34] respectively, and there is no Fe^{2+} formed under the given conditions.[35]

4.2. Influence of Cation Substitution. In general, the reactivity of a metal oxide with an acidic gas, CO_2, can be reflected by its (Lewis) acidity, leaving alone other effects (e.g., structure and stoichiometry). Higher acidity of the metal oxide corresponds to better resistance to CO_2. The relative acidity of a metal oxide can be derived using the Sanderson's electronegativity and the valence state of the cation.[36,37] The following acidity order of the metal oxides has been reported,[37] if represented by their respective cations: $Nb^{5+} > Co^{4+} > Co^{3+} > Fe^{3+} > Co^{2+} > Fe^{2+}$. Although the data for Fe^{4+} is unavailable in the literature, its acidity can be expected to be between that of Co^{3+} and of Co^{4+}.[36,37] The better CO_2 resistance resulting from substitution of Nb for Fe in the Co-free $BaCo_{1-x-y}Fe_xNb_yO_{3-\delta}$ is, therefore, consistent with the higher acidity of Nb^{5+} relative to the lower-valent iron cation.[37] In oxygen-deficient perovskite oxides, iron adopts a higher valence state (3+, 4+) than cobalt (2+, 3+) under the conditions concerned in the present work.[35,38,39] Furthermore, recent XANES (X-ray absorption near-edge spectroscopy) measurements carried out by the authors revealed that the valence states of both the iron and cobalt do not vary significantly with the iron content in $BaCo_{1-x-y}Fe_xNb_yO_{3-\delta}$ ($y = 0.2$). Therefore, Fe substitution for Co in this perovskite results in higher acidity and enhancement of its CO_2 resistance. On the other hand, the higher valence of niobium and iron cations, as well as their stronger attraction toward the binding oxygen atom (larger acidity), will lead to increase in the oxygen stoichiometry of the perovskite. It has been suggested that oxygen vacancies play an important role in the carbonate formation on $LaFeO_3$.[40] A decrease of oxygen vacancy concentration may, on the one hand, also enhance the acidity[41] and, on the other hand, help stabilize the perovskite structure,[28] both of which may contribute to enhancement of CO_2 resistance. One disadvantage of the reduction in the oxygen nonstoichiometry, however, is a decrease of the oxide ion conductivity and, hence, a decrease of the oxygen permeability of $BaCo_{1-x-y}Fe_xNb_yO_{3-\delta}$ with increasing Fe/Nb content.[42,43]

The stability of perovskite oxides in CO_2 may also be reflected by their lattice energy, a measure of the bonding in crystalline ionic compounds. However, such data are

(33) Tezuka, K.; Henmi, K.; Hinatsu, Y.; Masaki, N. M. *J. Solid State Chem.* **2000**, *154*, 591.
(34) Gibb, T. C. *J. Mater. Chem.* **1993**, *3*, 441.
(35) Teraoka, Y.; Yoshimatsu, M.; Yamazoe, N.; Seiyama, T. *Chem. Lett.* **1984**, 893.
(36) Sanderson, R. T. *Inorg. Chem.* **1986**, *25*, 3518.
(37) Jeong, N. C.; Lee, J. S.; Tae, E. L.; Lee, Y. J.; Yoon, K. B. *Angew. Chem., Int. Ed.* **2008**, *47*, 10128.
(38) Mueller, D. N.; De Souza, R.; Brendt, J.; Samuelis, D.; Martin, M. *J. Mater. Chem.* **2009**, *19*, 1960.
(39) Harvey, A. S.; Litterst, F. J.; Yang, Z.; Rupp, J. L. M.; Infortuna, A.; Gauckler, L. J. *Phys. Chem. Chem. Phys.* **2009**, *11*, 3090.
(40) Corberan, V. C.; Tejuca, L. G.; Bell, A. T. *J. Mater. Sci.* **1989**, *24*, 4437.
(41) Maier, J. *Chem.–Eur. J.* **2001**, *7*, 4762.
(42) Stevenson, J. W.; Armstrong, T. R.; Carneim, R. D.; Pederson, L. R.; Weber, W. J. *J. Electrochem. Soc.* **1996**, *143*, 2722.
(43) Teraoka, Y.; Zhang, H. M.; Okamoto, K.; Yamazoe, N. *Mater. Res. Bull.* **1988**, *23*, 51.

not available in the literature for the oxygen-deficient perovskites concerned. It should be noted that the calculation of lattice energy requires knowledge of parameters such as electron/coordination configuration and valence state of the B-site cations,[44] which readily vary with operation conditions like temperature and oxygen partial pressure and are usually undetermined for this kind of materials.[38]

The acidic, high-valent niobium has proven to be an effective B-site dopant for improving the CO_2 resistance of Ba(Co, Fe, Nb)$O_{3-\delta}$. Likewise, other high-valent cation dopants of similar ionic radius may be utilized, such as Ti, W, and Mo.[37] The CO_2 resistance may also benefit from substitution of the A-site cation, barium, by other alkaline earth or rare earth elements of higher acidity.[37] This strategy, in fact, is consistent with the several examples of materials design with improved CO_2 resistance reported so far, such as Ti-doped Sr(Co,Fe)$O_{3-\delta}$,[26] (Sr, Mo)-doped $BaFeO_{3-\delta}$[45] and Zr-doped Ba(Ce,Y)$O_{3-\delta}$.[23]

4.3. Implications. The instantaneous decrease of oxygen permeation flux of BCFN442 perovskite membrane upon exposure to CO_2, as shown in Figure 1, which has also been observed in other related materials,[7,12,13] is clearly linked with the instantaneous formation of the nonporous $BaCO_3$ on the membrane surface (Figure 4a). Once the $BaCO_3$ is formed, the underneath membrane surface is blocked from releasing any oxygen that is permeated from air to the sweep side of the membrane, thus leading to depression or even complete cessation of the oxygen permeation process. It is also worth while noting that the oxygen permeation flux degrades in CO_2 much more slowly at 1000 °C than at the lower temperatures in Figure 1, which can be simply explained as a result of the entropy-decreasing nature of the reaction between CO_2 and BCFN442 (cf. eq 3).

In terms of implementation of perovskite membranes in a 4-end oxy-fuel process,[6] a high oxygen permeation flux as well as sufficient stability in a CO_2 atmosphere is required. The trade-off between the performance and CO_2 resistance, which was observed not only for Ba(Co, Fe, Nb)$O_{3-\delta}$ but also for other perovskites,[23,26] however, may force one to use less-permeable materials. The reduced oxygen permeation flux may be compensated by a different membrane geometry that allows for thinner membranes, such as a hollow fiber membrane.[1] It is also important to note that, as inferred from eq 3, in order to prolong the service lifetime of a membrane in oxy-fuel combustion process, reducing the contents of O_2 and CO_2 in the flue gas, as well as raising the operation temperature, is beneficial with respect to CO_2 corrosion resistance. However, this may not meet the requirements of the oxy-fuel process. The flue gas also contains a significant amount of H_2O other than CO_2, which may add to the stringent stability requirements for the membranes. Degradation of structure and performance in the presence of H_2O, particularly in its copresence with CO_2, has been reported for other perovskite membranes.[7,15]

5. Conclusions

The degradation of both the performance and (micro)-structure of $BaCo_{0.4}Fe_{0.4}Nb_{0.2}O_{3-\delta}$ oxygen separation membrane in CO_2-containing atmospheres was investigated. The oxygen permeability deteriorates significantly upon exposure of the membrane to CO_2 in the sweep gas. This effect becomes more pronounced at lower temperatures. Reaction of the membrane with CO_2 leads to decomposition of the membrane material and formation of a compact $BaCO_3$ surface layer as well as a porous decomposed zone; the latter consists of mainly CoO and a Co-depleted perovskite phase. The composition of the perovskite product varies with depth in the decomposed zone, characterized by severe cobalt depletion close to the carbonate layer. The cobalt depletion is associated with reduction in the Ba^{2+} chemical potential of the perovskite. The growth kinetics of the product layers was found to follow a parabolic rate law, indicating a diffusion-controlled process. Increase in the partial pressure of CO_2 or O_2 results in faster membrane degradation. This observation, together with the fact that the $BaCO_3$ layer grows outward, may imply that diffusion of barium dominates the membrane degradation. Substitution of Fe for Co and of Nb for Fe in the perovskite leads to improved CO_2 resistance, which may be attributed to an increase of both the oxygen nonstoichiometry and oxide acidity. The degradation mechanism and strategy of material improvement proposed for $BaCo_{0.4}Fe_{0.4}Nb_{0.2}O_{3-\delta}$ may also be valid for other related perovskite-structured membranes.

Acknowledgment. Financial support for the joint research project MEM-OXYCOAL by the German Federal Ministry of Economics and Technology (BMWi) is gratefully acknowledged. J.Y. thanks Prof. M. Martin for fruitful discussions and Mr. D. Roehrens for assistance in the XRD measurements and analyses.

Supporting Information Available: Details of sample preparation, X-ray diffraction, and oxygen permeation measurements; additional figures as noted in the text (PDF). This material is available free of charge via the Internet at http://pubs.acs.org.

Note Added after ASAP Publication. Due to a production error, this paper published ASAP October 28, 2010, with an incorrect version of Figure 1; the paper with the correct version of Figure 1 was published ASAP on October 29, 2010, but contained an incorrect version of Figure 9. The paper with the correct Figure 9 was published ASAP November 3, 2010.

(44) Ishigaki, T.; Nikolic, Z. S.; Watanabe, T.; Matsushita, N.; Yoshimura, M. *Solid State Ionics* **2009**, *180*, 475.
(45) Dong, X. L.; Jin, W. Q.; Xu, N. P. *Chem. Mater.* **2010**, *22*, 3610.